

# Geometry-related magnetic interference patterns in long *SNS* Josephson junctions

F. Chiodi,<sup>1</sup> M. Ferrier,<sup>1</sup> S. Guéron,<sup>1</sup> J. C. Cuevas,<sup>2</sup> G. Montambaux,<sup>1</sup> F. Fortuna,<sup>3</sup> A. Kasumov,<sup>1</sup> and H. Bouchiat<sup>1</sup>

<sup>1</sup>*Laboratoire de Physique des Solides, UMR 8502, CNRS, Université Paris-Sud, 91405 ORSAY Cedex, France*

<sup>2</sup>*Departamento de Física Teórica de la Materia Condensada, Universidad Autónoma de Madrid, 28049 Madrid, Spain*

<sup>3</sup>*Centre de Spectrométrie Nucléaire et de Spectrométrie de Masse, UMR 8609, CNRS, Université Paris-Sud, 91405 ORSAY Cedex, France*

(Received 19 January 2012; revised manuscript received 20 July 2012; published 9 August 2012)

We have measured the critical current dependence on the magnetic flux of two long *SNS* junctions differing by the normal wire geometry. The samples are made by a Au wire connected to W contacts, via focused ion beam assisted deposition. We could tune the magnetic pattern from the monotonic Gaussian-like decay of a quasi-one-dimensional (1D) normal wire to the Fraunhofer-like pattern of a square normal wire. We explain the monotonic limit with a semiclassical 1D model, and we fit both field dependencies with numerical simulations of the two-dimensional Usadel equations. Furthermore, we observe both integer and fractional Shapiro steps. The magnetic flux dependence of the integer steps reproduces as expected that of the critical current  $I_c$ , while fractional steps decay slower with the flux than  $I_c$ .

DOI: 10.1103/PhysRevB.86.064510

PACS number(s): 74.45.+c, 73.23.-b, 74.40.Gh

## I. INTRODUCTION

A nondissipative supercurrent can be transmitted between two superconductors (*S*) through a nanometer-thin insulating layer (*I*), when a phase difference is imposed. Superconducting correlations can also penetrate into a micrometer-long, nonsuperconducting coherent metal (*N*) over lengths  $L$  greater than  $\xi_S$ , the superconducting coherence length in *N*. A supercurrent can then flow through long ( $L > \xi_S$ ) *SNS* junctions, provided that the phase coherence is preserved in the normal wire. The supercurrent amplitude only depends on the normal metal resistance, the normal metal length  $L$ , and diffusion coefficient  $D$ ,<sup>1</sup> the latter setting the diffusion time through the *N* wire  $\tau_D = L^2/D$ . The supercurrent thus reflects the transport mechanisms in the normal wire, and is affected by the interference and diffraction phenomena present in the normal metal as a result of the phase coherence. The characteristic energy of the junction is the Thouless energy, also set by the same parameters:  $E_{Th} = \hbar/\tau_D = \hbar D/L^2$ . The Thouless energy not only controls the supercurrent, but also determines the amplitude of the minigap  $\tilde{\Delta}_{\max} \approx 3.1E_{Th}$  created in the density of states of the normal wire by the proximity of the two superconducting contacts. In contrast to the superconducting gap  $\Delta$ , the minigap is fully modulated by the phase difference  $\Delta\varphi$  across the normal wire, being maximum at  $\Delta\varphi = 0$  and closing completely at  $\Delta\varphi = \pi$ .

We have studied the behavior of the supercurrent in long *SNS* junctions in a magnetic field perpendicular to the sample plane. In a previous work,<sup>2</sup> we observed that the maximum supercurrent, the critical current  $I_c$ , monotonously decreased with the magnetic field following a quasi-Gaussian dependence. This behavior is different from the interference Fraunhofer pattern usually observed, for example, in *SIS* junctions, *SNS* junctions with  $L \leq \xi_S$ , magnetic *SFS* Josephson junctions, etc. This difference is induced by the different aspect ratios of short weak links and long *SNS* junctions. Indeed, in *SIS* junctions the thickness of the junction is limited to a few angstroms, to permit the tunneling of Cooper pairs; similarly, in *SFS* junctions the magnetic layer thickness has to be shorter than a few tens of nanometers, so that Cooper pairs are not broken by the internal exchange field. In contrast to the wide

and short *SIS* and *SFS* junctions, *SNS* junctions offer the interesting possibility to explore a broad range of aspect ratios, since the length of the normal metal is only limited by the phase coherence length, which can be as long as a few micrometers at low temperature. In this paper we explore different geometries of long *SNS* junctions. Both monotonic and nonmonotonic  $I_c(B)$  dependencies have been observed before, but we show that we can tune the  $I_c(B)$  curve from an interference pattern to a quasi-Gaussian monotonic dependence by varying the normal metal's aspect ratio.

Monotonic  $I_c(B)$  dependencies have been observed in ballistic long *SNS* junctions, formed by a normal bidimensional InAs electron gas connected to superconducting Nb contacts larger than the London screening length.<sup>3</sup> Their magnetic field dependence resulted from the screening currents in the Nb. On the contrary, the diffusive junctions investigated in the present work are contacted by thin disordered superconducting wires in which the magnetic field screening is negligible. We show that the geometry-dependent magnetic field decay can be explained taking into account only the interferences between Andreev pairs' trajectories in the normal metal.

As a reminder, we first consider the case of a wide short *SIS* junction. A magnetic field in the *SIS* junction plane penetrates in the insulating layer of thickness  $d$  and in the superconductors nearby over a length  $\lambda_L$ , the London penetration length. In a magnetic field  $\vec{B} = -B\hat{z}$  of vector potential  $\vec{A} = By\hat{x}$ , the phase shift of the Cooper pairs tunneling at different points of the junction width is [Fig. 1(c)]

$$\theta(y) = 2\pi \frac{2e}{h} \int_{-\lambda_L}^{d+\lambda_L} A_x dx = 2\pi \frac{\Phi(y)}{\Phi_0}, \quad (1)$$

where  $\Phi(y)$  is the flux through the surface  $S_y = (d + 2\lambda_L)y$  and  $\Phi_0 = h/(2e)$  is the quantum flux. The current is obtained by integrating over the junction surface the supercurrent density  $j = j_c \sin(\delta + \theta)$ , taking into account both the superconducting phase difference between the contacts  $\delta$  and the phase due to the vector potential. The critical current dependence on the magnetic flux  $\Phi = B(d + 2\lambda_L)w$ , follows the well-known Fraunhofer pattern, a diffraction pattern created by the interference between the ballistic trajectories

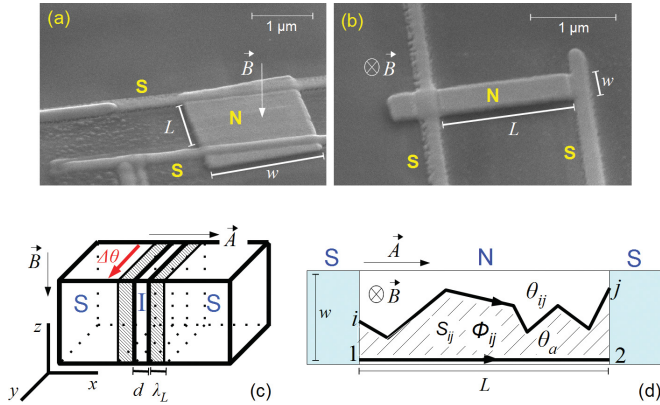


FIG. 1. (Color online) Scanning electron microscope images of samples WAU-Sq (a) and WAU-N (b). One can see as a clear halo the W contamination around the superconducting contacts. (c) Scheme of a *SIS* Josephson junction. (d) Scheme of the 1D model developed.

over the junction width:

$$I_c = I_c(0) \frac{\Phi_0}{\pi \Phi} \left| \sin \left( \frac{\pi \Phi}{\Phi_0} \right) \right|. \quad (2)$$

If we now consider *SNS* junctions, we expect strong differences between junctions containing a wide or a narrow normal wire of similar lengths: in the wide wire the phase difference between the trajectories comes from the phase distribution along the junction width, while in the narrow wire, the phase of each trajectory is mainly accumulated along the junction length.

## II. THE SAMPLES

We have fabricated long *SNS* junctions where a Au normal wire links two superconducting W contacts. First, a 50-nm-thick Au wire is drawn by *e*-beam lithography and deposited onto a SiO<sub>2</sub> substrate. We use 99.9999% pure gold, with a content in magnetic impurities (Fe) smaller than 0.1 ppm. This ensures a long phase coherence length  $L_\phi \sim 10 \mu\text{m}$  below 50 mK, measured in a separated weak localization experiment. We then deposit the superconducting contacts in a focused ion beam (FIB). After slightly etching the Au wire with the FIB to remove possible impurities on its surface, we inject a metallo-organic vapor of tungsten hexacarbonyl over the sample. This vapor is decomposed by the focused Ga<sup>+</sup> ion beam, and a disordered W alloy is deposited on the substrate. The wires produced are composed of tungsten, carbon, and gallium in varying proportions (in our case, the atomic concentrations are roughly 30% W, 50% C, and 20% Ga).<sup>4</sup> The superconducting critical temperature of the wires produced is  $T_c \sim 4$  K, an order of magnitude higher than the bulk  $T_c$  of W.<sup>5</sup> This could be due to the inclusion of Ga, which is itself a superconductor with  $T_c = 1$  K. The critical magnetic field of the wires is also strikingly high: at 1 K,  $H_c = 7$  T.<sup>6</sup> The W wires are 200 nm wide and 100 nm thick. The dependence of the superconducting properties of these wires on the deposition conditions has been investigated in detail in Li *et al.*<sup>7</sup> The superconducting gap as well as the Abrikosov flux lattice have been studied by scanning tunneling microscopy experiments.<sup>8</sup> The investigation of proximity-

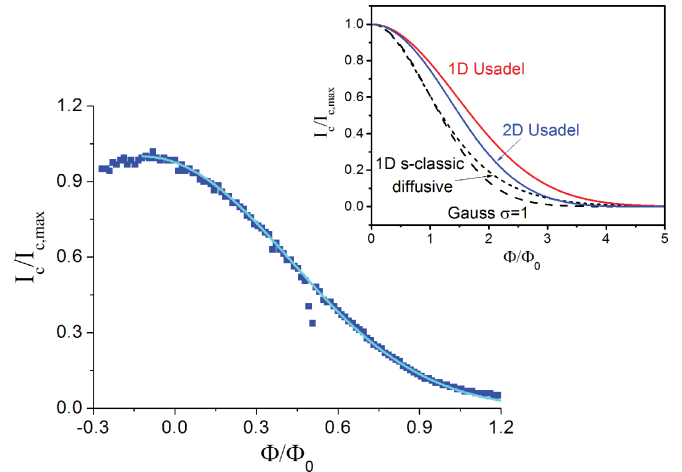


FIG. 2. (Color online) Main frame: sample WAU-N normalized critical current vs normalized flux at  $T = 60$  mK. Light blue line: numerical simulation of the 2D Usadel equations, where the flux has been rescaled by a factor of 2.5 to take into account an imperfect *S/N* interface. Inset: theoretical predictions for the aspect ratio of junction WAU-N and perfect interfaces: the analytical result of the Usadel equation in the 1D limit  $L \gg w$  (red line), the numerical simulation of the 2D Usadel equation (blue line), the semiclassical model for a 1D diffusive normal wire (dotted line), and a Gaussian curve with  $\sigma = 1$  in the notation of Eq. (7) (dashed line). The Gaussian best fit of the experimental data, which is also a good approximation of the numerical Usadel result, is obtained for  $\sigma = 0.5$  [as defined in Eq. (7)].  $I_{c,\text{max}} = 2.4 \mu\text{A}$ .

induced superconductivity in metallic nanowires contacted by FIB has also been recently performed.<sup>9</sup> The advantages of this technique are the deposition of the material of practically any shape and size, without any mask, and the good quality of the interface created. The main disadvantage is the Ga contamination of about 250 nm around the deposited wires. The *SNS* junctions created by FIB-assisted deposition are comparable to junctions created with more standard fabrication methods. We thus recovered the general results for the voltage vs current curves and the temperature dependence of the critical current.<sup>10</sup>

To investigate the influence of the geometry on the  $I_c(\Phi)$  dependence, we have designed two samples with different aspect ratios: sample WAU-Sq is  $1.2 \mu\text{m}$  long and  $1.75 \mu\text{m}$  wide, with an aspect ratio  $L/w = 0.7$ , while sample WAU-N is  $1.53 \mu\text{m}$  long and  $0.34 \mu\text{m}$  wide, with an aspect ratio  $L/w = 4.5$  [Figs. 1(a) and 1(b)].

The  $I_c(\Phi)$  normalized curves for samples WAU-N and WAU-Sq are shown in Figs. 2 and 3, respectively. They illustrate the important role of the aspect ratio: sample WAU-N displays a quasi-Gaussian decay of the critical current, while sample WAU-Sq displays oscillations which recall a Fraunhofer pattern.

## III. SEMICLASSICAL MODEL

To explain the behavior of sample WAU-N, a semiclassical model was developed.<sup>11</sup> The aim is to model a long diffusive *SNS* junction, with  $w \ll L \ll L_\phi, L_T$  (1D geometry), in a perpendicular magnetic field  $\vec{B} = -B\hat{z}$  of vector potential

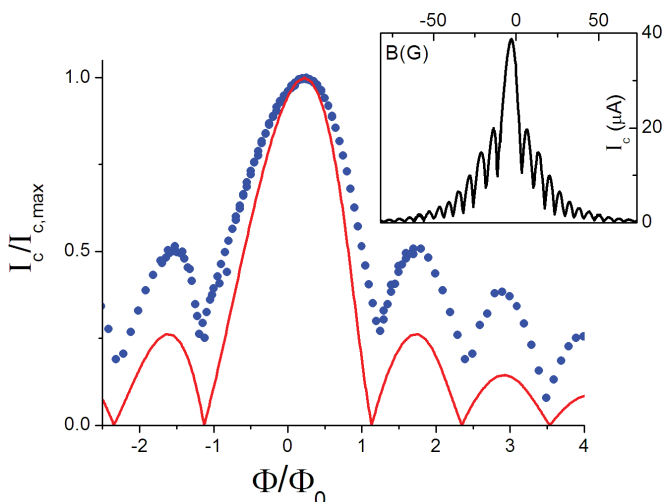


FIG. 3. (Color online) Sample WAU-Sq normalized critical current vs normalized flux at  $T = 60$  mK (blue dots). A trapped flux of 4.3 G has been subtracted. Red line: numerical simulation of the 2D Usadel equation for a junction with aspect ratio  $L/w = 0.7$  and W wires inductance  $\mathcal{L} = 11.5$  pH. Inset: raw data for  $I_c(B)$ , with  $I_{c,\max} = 38.8$   $\mu\text{A}$ .

$\vec{A} = By\hat{x}$  [Fig. 1(d)]. We suppose a sinusoidal current-phase relation for simplicity:  $j = j_c \sin(\delta + \theta_{ij})$ .  $\theta_{ij}$  is the phase acquired along the trajectory starting at point  $i$  and finishing at point  $j$ .  $\delta$  is the phase difference between the two superconducting contacts, and is independent of the position of  $i$  and  $j$ , since in this 1D geometry one can ignore the dephasing along the junction width in comparison to the one along the junction length. The total current is the average over all possible trajectories  $C_{ij}$ :

$$I \propto \text{Im}[\langle e^{i(\delta+\theta_{ij})} \rangle_{C_{ij}}]. \quad (3)$$

Considering a reference trajectory 1–2 with a phase difference  $\theta_a$ , we have  $\theta_{ij} = \theta_a + \Delta\theta_{ij}$  [see Fig. 1(d)]. The critical current is the maximum of the current  $I$ :

$$I_c \propto \text{Im}[e^{i(\delta+\theta_a)} \langle e^{i\Delta\theta_{ij}} \rangle_{C_{ij}}]_{\max} \propto |\langle e^{i\Delta\theta_{ij}} \rangle_{C_{ij}}|. \quad (4)$$

Given the great number of possible trajectories, the central limit theorem sets the distribution of the trajectories length to a Gaussian distribution. The phase  $\theta_{ij}$ , associated with the trajectory  $ij$ , follows then also a Gaussian distribution. Thus

$$I_c \sim \left| e^{-1/2 \langle (\Delta\theta_{ij})^2 \rangle_{C_{ij}}} \right|, \quad (5)$$

where  $\Delta\theta_{ij} = \theta_{ij} - \theta_a$  is proportional to the flux  $\Phi_{ij}$  in the surface  $S_{ij}$  defined by the trajectory  $ij$  [Fig. 1(d)]:

$$\begin{aligned} \Delta\theta_{ij} &= \frac{2e}{\hbar} \left[ \int_i^j A_x dx - \int_1^2 A_x dx \right] \\ &= \frac{2e}{\hbar} \oint A_x dx = 2\pi \frac{\Phi_{ij}}{\Phi_0}. \end{aligned} \quad (6)$$

Introducing Eq. (6) in Eq. (5), we find that the critical current decays as a Gaussian function:

$$I_c \sim \left| e^{-(\Phi/\Phi_0)^2 / (2\sigma^2)} \right|, \quad (7)$$

where  $\sigma^2 = [S^2 / \langle S_{ij}^2 \rangle_{C_{ij}}] / (4\pi^2)$  and  $S = w \times L$ . The Gaussian fit of sample WAU-N gives  $\sigma = 0.5$ , while in our previous

results,<sup>2</sup> we obtained  $\sigma$  in the range 0.74–1.8 for aspect ratios  $L/w$  in the range 1.9–10.4.

Beyond this simple Gaussian approximation, the exact calculation describing diffusive trajectories from point  $i$  to point  $j$  gives<sup>11</sup>

$$I_c = I_c(0) \frac{\frac{\pi}{\sqrt{3}} \frac{\Phi}{\Phi_0}}{\sinh\left(\frac{\pi}{\sqrt{3}} \frac{\Phi}{\Phi_0}\right)}. \quad (8)$$

The small difference between this flux dependence and a Gaussian one is shown in the inset of Fig. 2. While this model explains the origin of the quasi-Gaussian shape of our  $I_c(\Phi)$  curves, the experimental decay is faster than the predicted one. A more precise calculation, taking into account the two-dimensional (2D) nature of both samples as well as the role of imperfect interfaces, is thus necessary.

#### IV. USADEL EQUATIONS

Cuevas and Bergeret<sup>12</sup> have solved the 2D Usadel equation for long diffusive  $SNS$  junctions with low-resistance interfaces and for different aspect ratios of the normal wire. A complete field penetration in the normal metal ( $w < \lambda_{L,N}$ ) is assumed, neglecting any Josephson current screening effects. Moreover no inelastic scattering is considered. The authors found different limits:

(1)  $w \ll L$ : In this 1D limit, Usadel equations can be solved analytically yielding a monotonous Gaussian decay of the flux-dependent critical current: at  $T = 0$ ,  $I_c(B)/I_c(0) \sim e^{-0.238(\Phi/\Phi_0)^2}$  (inset of Fig. 2).

(2)  $w \leq L$ : The analytical expression being no longer valid, a numerical solution of the Usadel equations needs to be found. However, the numerical simulation still yields a monotonous quasi-Gaussian decay of  $I_c$  with the flux.

(3)  $w \gg L$ : In this case, the main effect of the field is to modulate the phase over the junction width, giving rise to an interference pattern, which is identical to a Fraunhofer pattern for small enough aspect ratios ( $L/w < 0.04$ ).

The authors do not suppose a purely sinusoidal current-phase relation to start with, but calculate the complete  $I(\delta)$  relation of a long  $SNS$  junction. However, the wide junction limit corresponds exactly to the Fraunhofer pattern obtained in the case of a sinusoidal current-phase relation.

#### V. EXPERIMENTAL RESULTS

In agreement with the prediction of Cuevas *et al.* for the aspect ratio  $L/w = 4.5$ , junction WAU-N does not exhibit any oscillating pattern (Fig. 2). The field decay cannot, however, be fitted by the numerical simulation for the corresponding flux scale  $\Phi/\Phi_0$ : the experimental decay is faster than the predicted one by a factor of 2.5. This can be explained by taking into account a nonperfect interface,<sup>13</sup> with an interface resistance  $R_i$  given roughly by  $R_i = 2R_N \sim 5 \Omega$  (the ratio  $R_i/R_N = 2$  leads to a rescaling of the perfect interface curve by a factor of 2.3). The main effect of nonideal interfaces is indeed to increase the dwell time in the normal metal of the coherent pairs carrying the supercurrent, thereby leading to a larger enclosed flux. In the case of sample WAU-N, this nonperfect interface may be attributed to the right W contact,

which is just at the extremity of the gold wire [see the scanning electron microscopy image, Fig. 1(b)].

To understand the experimental  $I_c(\Phi)$  of sample WAu-Sq, it is necessary to take into account not only the aspect ratio of the normal wire, but also the flux correction due to the inductance of the W contacts, evident in the tilt of the central peak of the  $I_c(\Phi)$  curve. The “internal” flux  $\Phi_{\text{int}}$  through the normal wire is thus the sum of the applied external flux  $\Phi$  and the flux created by the current flowing in the superconducting contacts,  $\Phi_{\mathcal{L}} = \mathcal{L} \times I_c(\Phi_{\text{int}})$ , following the relation

$$\Phi_{\text{int}} = \Phi + \mathcal{L} I_c(\Phi_{\text{int}}). \quad (9)$$

The experimental curve should then be compared not to the calculated curve  $I_c^{\text{th}}(\Phi_{\text{int}})$  but to  $I_c^{\text{th}}(\Phi) = I_c^{\text{th}}[\Phi_{\text{int}} - \mathcal{L} I_c^{\text{th}}(\Phi_{\text{int}})]$ . The best fit of our data for sample WAu-Sq according to the above expression yields  $\mathcal{L} = 11.5$  pH. This value, which we attribute to the kinetic inductance (much larger than the geometrical one) of the two 2- $\mu\text{m}$ -long superconducting wires over the normal metal, is compatible with the kinetic inductance of similarly made W wires.

When comparing our experimental results with the numerical simulation of the 2D Usadel equation for  $L/w = 0.7$  modified by the self-inductance, we find good agreement in the position of the zeros for  $\Phi = BS$ , with  $S = 3.25$   $\mu\text{m}^2$ . This corresponds roughly to the whole surface of the normal metal square, slightly larger than the surface between the contacts. The amplitude of the measured oscillations following the central peak decreases slower than predicted, and the minima of the first periods do not go to zero; this can be qualitatively explained as the effect of a nonuniform current distribution in the normal metal.<sup>14</sup>

## VI. SHAPIRO STEPS

We have measured the differential resistance  $dV/dI$  when irradiating the junctions with microwaves from an antenna. We have observed Shapiro steps, in the form of microwave-induced zero resistance dips at  $V = \frac{h}{2e} n f$ . They result from the resonance of the ac voltage at frequency  $f$  induced by the microwaves, with the current oscillations at frequency  $f_J = 2$  eV/h, due to the ac Josephson effect at finite voltage  $V$  [Figs. 4(a) and 4(b)]. In addition to the Shapiro steps at integer  $n$ , we find fractional Shapiro steps at  $n = 1/2, n = 1/3, n = 3/2$ , and  $n = 1/4$ . In contrast to what has been observed by Dubos<sup>15</sup> at high temperature ( $T = 4$  K, corresponding to  $13E_{Th}$ ), at  $T = 150$  mK ( $2.4E_{Th}$ ) we still see Shapiro steps with  $n > 1$  at voltages larger than the Thouless energy ( $E_{Th}/e = 5.3$   $\mu\text{V}$ ). Moreover, we observe Shapiro steps for frequencies larger than the minigap ( $\tilde{\Delta}/h = 4$  GHz), despite the fact that frequencies of the order of the minigap are expected to break the pairs and create excitations above the minigap.

Fractional Shapiro steps appear in  $SNS$  junctions as a consequence of a nonsinusoidal current-phase relation. The additional harmonics in the current-phase relation can be generated by multiple coherent Andreev reflexions (MAR), when the coherence length is much longer than the  $N$  length, or by nonequilibrium effects. Fractional Shapiro steps reflect the behavior of each harmonic individually: the step at  $n = 1/2$ , for example, is generated by the second harmonic and is

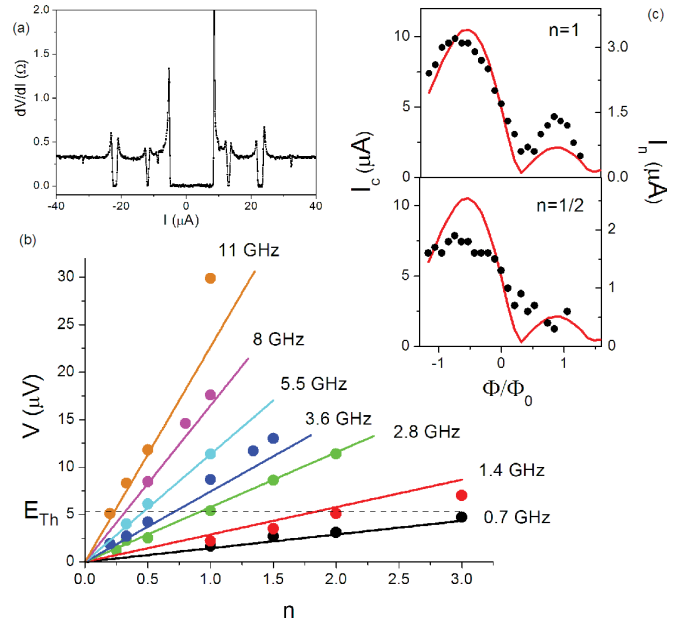


FIG. 4. (Color online) (a) Differential resistance  $dV/dI$  of sample WAu-Sq in the presence of an irradiation at frequency  $f = 2.8$  GHz. (b) dc voltage vs Shapiro step order for sample WAu-Sq; the voltage was directly deduced from the measured  $V(I)$  curves. Lines show the predicted dependence  $V = h/2en f$ . (c) Normalized flux dependence of Shapiro steps current amplitude for  $n = 1$  and  $n = 1/2$  (symbols) compared to the critical current dependence under microwaves, which cause the reduction in  $I_c$  amplitude (continuous lines); the trapped flux of 4.3 G, corresponding to  $0.7 \Phi_0$ , is partially compensated by the inductance-related tilt of the  $I_c(\Phi)$  central peak.

proportional to its amplitude, having the same dependence on field and temperature. We have studied the magnetic field dependence of both integer and fractional step amplitudes. As expected, the field dependence of the integer Shapiro steps follows roughly that of the zeroth-order step, the critical current [Fig. 4(c)]. This is not the case, however, for the fractional steps: In Fig. 4 we show that the decay with the normalized flux of step  $n = 1/2$  is slower than that of the critical current. If this fractional Shapiro step was due to the MAR at equilibrium, the field dependence would show a periodicity half that of the critical current, corresponding to the double length covered by the Andreev pairs, and the zeros of the Fraunhofer pattern should be found at multiples of  $\Phi_0/2$ . This is evidently not the case, so that the supplementary harmonic in the current-phase relation may be traced back to nonequilibrium effects, as already suggested in Dubos *et al.*<sup>15</sup> and Chiodi *et al.*<sup>16</sup> Moreover, the effect of the magnetic field at the lowest temperatures was already shown to increase the total critical current in the out-of-equilibrium  $SNS$  junction.<sup>17</sup>

## VII. CONCLUSIONS

We have measured the  $I_c(\Phi)$  curves for two different geometries of long  $SNS$  junctions. The samples are made by a Au wire connected to W contacts, via FIB-assisted deposition. We have observed a monotonic Gaussian-like

decay for a quasi-one-dimensional normal wire, in contrast to the Fraunhofer-like interference pattern of a square normal wire. We explain the monotonic limit with a semiclassical 1D model, and fit both field dependencies with numerical simulations of the 2D Usadel equation. Moreover, we have observed both integer and fractional Shapiro steps and their dependence in magnetic field. While integer steps follow as expected the field dependence of the critical current, fractional steps decay slower than  $I_c$ . This is incompatible

with equilibrium MAR-originated steps, but may be explained as an out-of-equilibrium effect.

#### ACKNOWLEDGMENTS

We are grateful to M. Aprili, R. Deblock, B. Reulet, A. Chepelianskii, J. Gabelli, and I. Petkovic for fruitful discussions. This work was supported by RTRA Triangle de la Physique NanoMan and ANR QuantADN.

<sup>1</sup>T. T. Heikkilä, J. Särkkä, and F. K. Wilhelm, *Phys. Rev. B* **66**, 184513 (2002).

<sup>2</sup>L. Angers, F. Chiodi, G. Montambaux, M. Ferrier, S. Guéron, and H. Bouchiat, J. C. Cuevas, *Phys. Rev. B* **77**, 165408 (2008).

<sup>3</sup>F. Rohlfing, G. Tkachov, F. Otto, K. Richter, D. Weiss, G. Borghs, and C. Strunk, *Phys. Rev. B* **80**, 220507 (2009).

<sup>4</sup>The concentrations are deduced with a 50% error by EDX measurement.

<sup>5</sup>W. L. Bond, A. S. Cooper, K. Andres, G. W. Hull, T. H. Geballe, and B. T. Matthias, *Phys. Rev. Lett.* **15**, 260 (1965).

<sup>6</sup>A. Yu. Kasumov, K. Tsukagoshi, M. Kawamura, T. Kobayashi, Y. Aoyagi, K. Senba, T. Kodama, H. Nishikawa, I. Ikemoto, K. Kikuchi, V. T. Volkov, Yu. A. Kasumov, R. Deblock, S. Guéron, and H. Bouchiat, *Phys. Rev. B* **72**, 033414 (2005).

<sup>7</sup>W. Li, J. C. Fenton, Y. Wang, D. W. McComb, and P. A. Warburton, *J. Appl. Phys.* **104**, 093913 (2008).

<sup>8</sup>I. Guillamon, H. Suderow, S. Vieira, A. Fernández-Pacheco, J. Sesé, R. Córdoba, J. M. De Teresa, and M. R. Ibarra, *New J. Phys.* **10**, 093005 (2008).

<sup>9</sup>J. Wang, C. Shi, M. Tian, Q. Zhang, N. Kumar, J. K. Jain, T. E. Mallouk, and M. H. W. Chan, *Phys. Rev. Lett.* **102**, 247003 (2009); J. Wang, M. Singh, M. Tian, N. Kumar, B. Liu, C. Shi, J. K. Jain, N. Samarth, T. E. Mallouk, and M. H. W. Chan, *Nat. Phys.* **6**, 389 (2010).

<sup>10</sup>P. Dubos, H. Courtois, B. Pannetier, F. K. Wilhelm, A. D. Zaikin, and G. Schon, *Phys. Rev. B* **63**, 064502 (2001).

<sup>11</sup>G. Montambaux, *arXiv:0707.0411*.

<sup>12</sup>J. C. Cuevas and F. S. Bergeret, *Phys. Rev. Lett.* **99**, 217002 (2007).

<sup>13</sup>J. C. Hammer, J. C. Cuevas, F. S. Bergeret, and W. Belzig, *Phys. Rev. B* **76**, 064514 (2007).

<sup>14</sup>Antonio Barone and Gianfranco Paternó, *Physics and Applications of the Josephson Effect* (Wiley, New York, 1982).

<sup>15</sup>P. Dubos, H. Courtois, O. Buisson, and B. Pannetier, *Phys. Rev. Lett.* **87**, 206801 (2001).

<sup>16</sup>F. Chiodi, M. Ferrier, K. Tikhonov, P. Virtanen, T. T. Heikkilä, M. Feigelman, S. Guéron, and H. Bouchiat, *Sci. Rep.* **1**, 3 (2011).

<sup>17</sup>F. Chiodi, M. Aprili, and B. Reulet, *Phys. Rev. Lett.* **103**, 177002 (2009).